

## Double-Shock Compression Pathways from Diamond to BC8 Carbon

Jiuyang Shi, Zhixing Liang, Junjie Wang, Shuning Pan, Chi Ding, Yong Wang,  
Hui-Tian Wang, Dingyu Xing, and Jian Sun<sup>\*</sup>

*National Laboratory of Solid State Microstructures, School of Physics and Collaborative Innovation Center of Advanced Microstructures, Nanjing University, Nanjing, 210093, People's Republic of China*

 (Received 17 May 2022; revised 11 July 2023; accepted 8 September 2023; published 6 October 2023)

Carbon is one of the most important elements for both industrial applications and fundamental research, including life, physics, chemistry, materials, and even planetary science. Although theoretical predictions on the transition from diamond to the BC8 ( $Ia\bar{3}$ ) carbon were made more than thirty years ago, after tremendous experimental efforts, direct evidence for the existence of BC8 carbon is still lacking. In this study, a machine learning potential was developed for high-pressure carbon fitted from first-principles calculations, which exhibited great capabilities in modeling the melting and Hugoniot line. Using the molecular dynamics based on this machine learning potential, we designed a thermodynamic pathway that is achievable for the double shock compression experiment to obtain the elusive BC8 carbon. Diamond was compressed up to 584 GPa after the first shock at 20.5 km/s. Subsequently, in the second shock compression at 24.8 or 25.0 km/s, diamond was compressed to a supercooled liquid and then solidified to BC8 in around 1 ns. Furthermore, the critical nucleus size and nucleation rate of BC8 were calculated, which are crucial for nano-second x-ray diffraction measurements to observe BC8 carbon during shock compressions. The key to obtaining BC8 carbon lies in the formation of liquid at a sufficient supercooling. Our work provides a feasible pathway by which the long-sought BC8 phase of carbon can be reached in experiments.

DOI: [10.1103/PhysRevLett.131.146101](https://doi.org/10.1103/PhysRevLett.131.146101)

Carbon is the fourth most abundant element in the universe and one of the key elements of life. Its allotropes with advanced properties have many important applications in scientific research and industry. For instance, graphene [1], fullerene ( $C_{60}$ ) [2], and carbon nanotubes [3] have shown superior performance and numerous potential applications in electronics, materials, and energy science. In particular, the diamondlike materials [4–8] with advanced mechanical properties were synthesized in the laboratory with high pressure method recently. Despite efforts to study high-pressure phases of carbon, the experimental evidence of these phases is lacking due to the remarkable stability of diamond over a wide pressure range. It has been reported that these phases may exist in the interior of carbon-rich planets, which are important for modeling them [9,10].

According to previous theoretical calculations [11–21], diamond will become energetically unstable at around 1 TPa and transform into the BC8 phase (space group:  $Ia\bar{3}$ ) [12,13], which is denser than diamond, and, in particular, metallic under high pressure, although with  $sp^3$  hybridization. The transition pressure from the BC8 phase to the SC1 phase is around 3 TPa [15,16]. Previous calculations [14] show that the transition barrier from diamond to BC8 carbon is about 2.5 eV/atom, which means that the diamond structure can persist to very high pressure during compression, as shown in the metadynamics simulations [21]. The metastability of diamond under terapascal was

also probed by a recent experiment [22]. To overcome such a high barrier, Sun *et al.* [21] designed a complicated pathway to obtain BC8 by decompression from the high-pressure SC1 phase. Recently, a machine learning potential has been used to simulate the formation of BC8 carbon with a billion atoms and nanosecond timescales [23]. However, the pathways discussed in these works [14,21,23] are still quite difficult for experiments. Therefore, a feasible direct pathway to obtain BC8 carbon from diamond is still unclear, although it is urgent and necessary.

From the experimental side, for pressures beyond a terapascal, the dynamic loading technologies [22,24–31] become essential. For instance, with the magnetically driven flyer-plate technique, a tiny discontinuity was obtained on the principal Hugoniot line of diamond, indicating the diamond-BC8-liquid triple point [25]. It has been reported that using decaying shock compression [27] and ramp compression [28], the maximum pressure of high-pressure experiments of carbon was increased from 1 to 5 TPa. However, structural measurements are still lacking in these experiments. Until a recent ramp compression experiment [22], the x-ray diffraction pattern indicated that solid carbon can retain the metastable diamond structure near 2 TPa.

While diamond was predicted to transform to the BC8 phase at around 1 TPa in 1987 [12,13], direct experimental evidence supporting its existence is still lacking. Therefore,

it is crucial to design an achievable transition path for dynamic compression experiments since this type of experiment is extremely difficult and expensive. To study phase transitions with such complex landscapes, simulations with sufficiently large systems and long timescales at an accuracy comparable to density functional theory (DFT) are necessary. Machine learning potentials can help balance the cost and accuracy of calculations, which have shown great performance in studying the complex behaviors of matter under extreme conditions recently [32–38].

In this study, we constructed a machine learning potential (MLP) for high-pressure carbon. The melting and Hugoniot line of carbon calculated by our MLP are consistent with the results from DFT and experiments. Using the MLP, we designed a double shock compression pathway to obtain BC8 carbon. Diamond was compressed to a supercooled liquid and then crystallized to BC8 phase in the double shock compression simulations. We also calculate the critical nucleus size and nucleation rate of BC8 which is an important constraint for nano-second X-ray diffraction experiments to observe BC8 carbon during shock compression.

To enable large-scale simulations of carbon under extreme conditions with the accuracy of quantum mechanics, we have constructed a MLP based on the neuro-evolution potential (NEP) framework that is fitted from first-principles calculations using the GPUMD package [39]. Our dataset contains 12 873 structures including different solid states, liquid states, solid-liquid interfaces, as well as many other systems, with the largest system consisting of up to 1,024 atoms. After sufficient iterative training, a final neural network was constructed to predict the energies and forces. The details about our DFT calculations and the constructions of our NEP potential can be found in the Supplemental Material [40].

We present a series of validation tests to evaluate the performance of our NEP machine learning potential. The first part of the validation test involves calculating the melting line of the diamond (FC8) and BC8 phases using the two-phase method [58]. As shown in Fig. 1(a), almost all the melting points calculated with DFT in this work (white squares) sit on the NEP melting lines (red thick lines), and the largest temperature error is around 200 K ( $\sim 3\%$ ). Our results also align well with the majority of previous theoretical studies [17–19,37,38], especially the recent work using machine learning potential [37,38], without exhibiting extreme deviations. Another important test for our NEP potential is to recover the principle Hugoniot line of the diamond, which is performed through a series of NVT simulations to find the points that satisfy the Hugoniot condition [19,59,60]. The NEP pressure-temperature Hugoniot line (blue thick lines) exhibits good agreement with the results calculated with SNAP MLP (orange dashed lines) [37], both in the solid and liquid portions of the Hugoniot line. When comparing the NEP

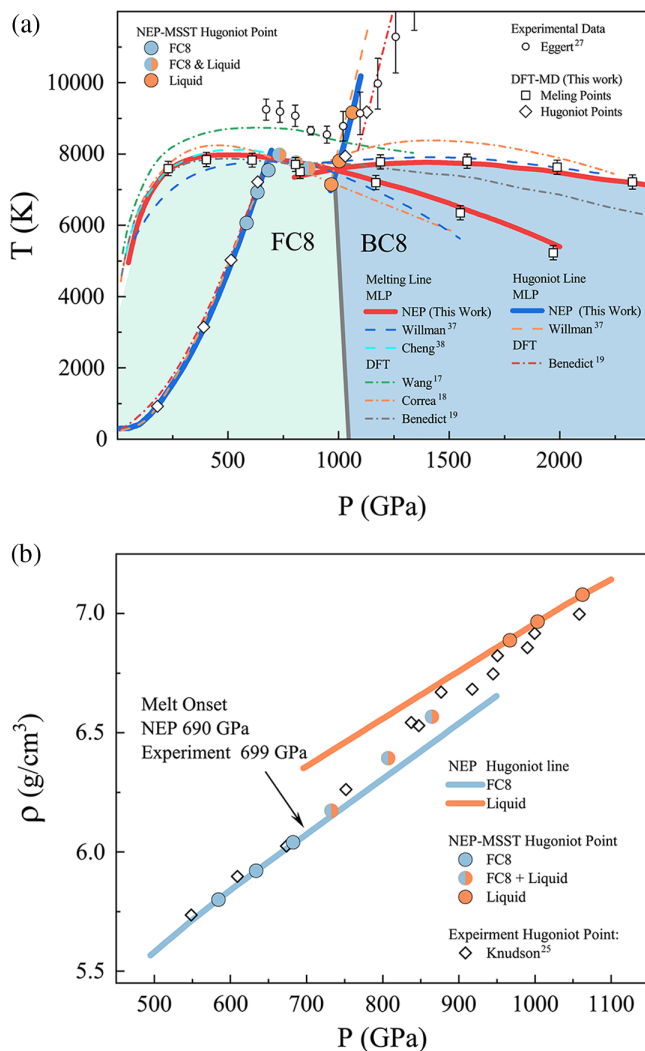


FIG. 1. The melting lines and points and Hugoniot lines and points calculated with NEP potential compared with our DFT results, previous calculations [17–19,37,38], and experiment data [25,27]. (a) The melting lines and points of diamond (FC8) and BC8 phase and pressure-temperature Hugoniot lines and points. (b) The pressure-density Hugoniot lines and points.

results with the DFT results from Benedict *et al.* [19] and our own DFT results, the solid portion of the Hugoniot line still exhibits good agreement. While some deviations are observed in the high temperature liquid portion, which might be attributed to the significant electronic entropy effect at high temperatures included in DFT calculations.

Although our results compare well with most theoretical results, there is still a gap with experimental measurements from Eggert *et al.* [27], using the decaying shock compression. Since the equilibrium of a phase transition to a well-defined shock state is hard to be achieved in the decaying shock compression experiment [29], we also compared the NEP pressure-density Hugoniot line with the experiment data of Knudson [25], as depicted in Fig. 1(b). The onset point of diamond melting measured

by shock compression experiments is around (699 GPa,  $6.08 \text{ g/cm}^3$ ), which was predicted to be around (690 GPa,  $6.05 \text{ g/cm}^3$ ) by our NEP simulations. The experiment Hugoniot points below 699 GPa sit on the solid part of the NEP Hugoniot line. Meanwhile, the experiment points higher than 699 GPa were located between the solid part and liquid part of the NEP Hugoniot line and gradually approached the liquid part as pressure increased. These results demonstrate the reliability of the NEP potential used in this study. Other validation tests can be found in the Supplemental Material [40].

To investigate the thermodynamic process and structural evolution during shock compression, we conducted nano-second-scale molecular dynamics simulations involving 212960 atoms with the multiscale shock technique (MSST) method [61–63]. The shock compressions were applied along the  $\langle 100 \rangle$  direction of the diamond. The MSST Hugoniot points were represented as solid dots in Fig. 1. The final states of the complete solid and liquid phases were aligned with the solid and liquid parts of the Hugoniot line, respectively. And the solid-liquid co-extensive points were situated on the melting line as a transitional section.

In the single shock compression simulations of diamond (FC8), the Hugoniot line approaches the FC8-BC8-liquid triple point in the phase diagram. Our single shock MSST simulations did not show any indication of the FC8-BC8 phase transformation. To explore feasible pathways for achieving the BC8 phase at higher pressures, we performed double-shock MSST simulations. As shown in Fig. 2, we set the velocity of the first shock at 20.5 km/s to compress

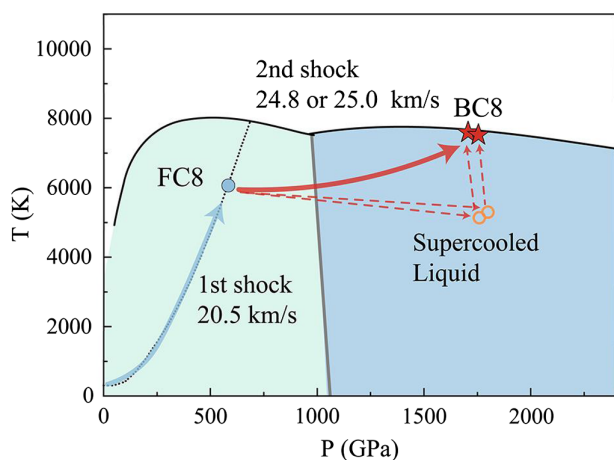


FIG. 2. The double shock compression pathway to get BC8 carbon. The first shock compression (blue solid arrow) was applied along the  $\langle 100 \rangle$  direction of the diamond at the velocity of 20.5 km/s. Then, the second shock compression (red solid arrow) was applied in the same direction. The phase transition processes during the second shock at 24.8 and 25.0 km/s are marked in the red dashed arrows.

the diamond to 584 GPa, and then applied a second shock along the same direction.

With the second shock at 24.8 and 25.0 km/s, the phase transition from FC8 to BC8 can be observed directly in our simulations. In Fig. 3, we presented the phase transition process during the second shock compression at 24.8 km/s. The local average atomic environment similarity was used to determine whether a local atomic environment is solidlike or liquidlike [40]. Within 10 ps, the diamond was compressed to a supercooled liquid state with ultrahigh density, and the pressure increased to around 1.75 TPa, which is within the stable pressure range of BC8 carbon. The temperature of the intermediate metastable liquid is around 5100 K, which is still much lower than the melting temperature of the BC8 phase (approximately 7600 K at 1.75 TPa). As time progressed, homogeneous nucleation occurred at around 394 ps releasing a significant amount of heat. After further growth of BC8 carbon, a clear and representative pattern of BC8 carbon can be observed, as shown in Fig. 3(e). The recrystallization phenomenon induced by shock has also been observed in the MSST shock compression simulations of  $\text{SiO}_2$  [63]. The phase transition process can be reflected in the simulated x-ray diffraction (XRD) patterns, as presented in Fig. 3(f). Four clear diffraction peaks can be observed in the simulated XRD patterns at 400 ps and the peak positions are in nearly perfect agreement with the BC8 phase, confirming the formation of BC8 carbon during our simulations.

Subsequently, we extended the range of shock velocities for the second shock to determine the range in which BC8 can form. As presented in Fig 4(a), the MSST Hugoniot line exhibits three distinct regions: diamond, diamond and liquid, and complete liquid. The detailed discussions about Fig 4(a) can be found in the Supplemental Material [40]. Here, we focused on the supercooled liquid part from which the BC8 phase can nucleate and grow. For the second shock compression at 24.8 or 25.0 km/s, a highly supercooled liquid is formed, enabling direct observation of BC8 nucleation due to the high nucleation rate. However, for the second shock with a higher velocity, the supercooled liquid is formed under higher temperatures (not highly supercooled), which makes it challenging to directly observe the nucleation of BC8 using normal MD simulations. To overcome the limitations of sampling rare events, we adopt the seeding method [64–67] to calculate the critical nucleus size and nucleation rate within the framework of classic nucleation theory [40].

In Fig. 4(b), we report the critical nucleus size and the nucleation rate of BC8 carbon at 1.8 and 2 TPa, respectively. Considering the limited observation time of nano-seconds for dynamic compression experiments and assuming a sample size of around  $1 \text{ mm}^3$ , the nucleation of BC8 with a rate lower than  $10^{18} \text{ m}^{-3} \text{ s}^{-1}$  ( $1 \text{ mm}^{-3} \text{ ns}^{-1}$ ) is nearly impossible to be observed. Our calculations indicate that the critical temperature corresponding to the

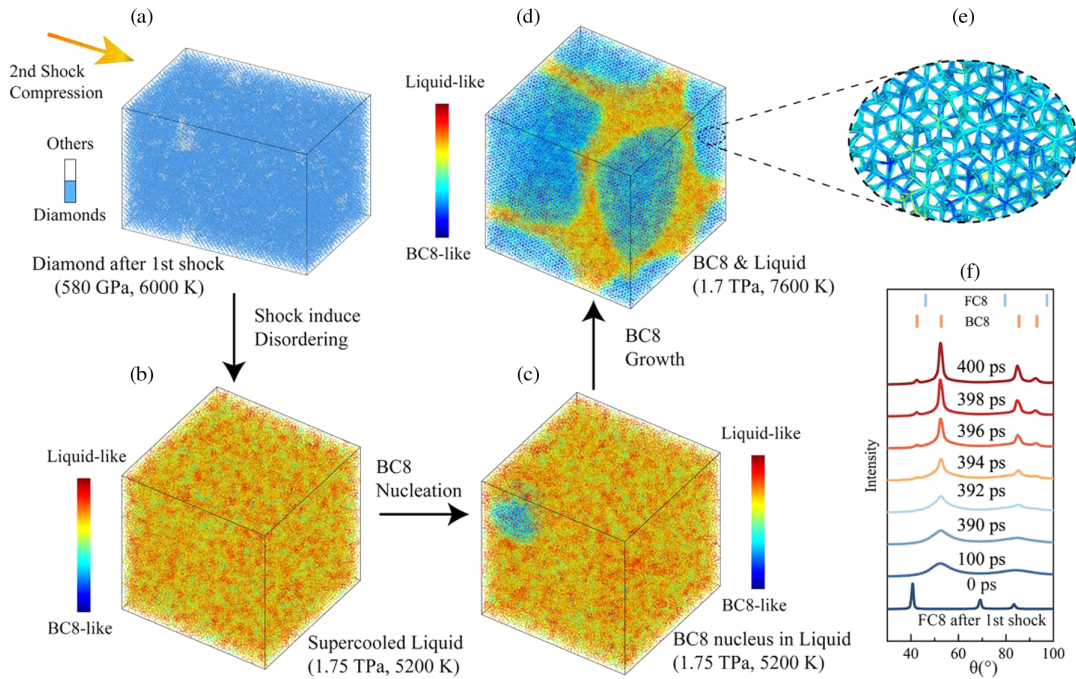


FIG. 3. The FC8-BC8 phase transition process during the second shock. (a)–(d) The structures viewed in different stages of the phase transition. (e) Representative patterns of the BC8 phase viewed along the  $\langle 111 \rangle$  direction. (f) The time evolutions of the calculated x-ray diffraction patterns during MD simulations with a wavelength of 0.5052 Å. The atoms type in the structure of (a) is classified using the polyhedral template matching method [79]. For the structure in (b)–(d), the atoms and bonds are colored by the value of  $(\bar{K}_{\text{BC8}} - \bar{K}_{\text{Liquid}})$ , see details in the Supplemental Material [40]. All the structures were drawn and rendered using OVITO [80].

nucleation rate of  $1 \text{ mm}^{-3} \text{ ns}^{-1}$  is around 6215 and 5915 K, respectively, at 1.8 and 2 TPa. Combining the results of double shock compression and nucleation rate calculation, we estimated that the reasonable shock velocity range for the second shock to observe the formation of BC8 is approximately from 24.8 to 25.6 km/s, as shown in Fig. 4(a).

Recently, the double-shock compression scheme has been successfully applied in experimental studies on the melting of MgO [68]. In addition, the multiple-shock compression experiments have been applied in several other systems, such as Fe [69] and  $\text{H}_2\text{O}$  [70]. Ramp compression [22,28,29] is another dynamic-loading technique, which compresses the sample slowly enough to avoid the occurrence of a shock wave and reach high pressure but lower temperature than shock compression. Recent ramp compression experiments [22] have verified that carbon can persist in the metastable diamond structure under 2 TPa. Our simulations show that in the shock compression, the diamond will transform into a supercooled liquid, and then crystallize into BC8. However, it seems that during the ramp compression experiment, no intermediate liquid state was formed and the phase transition to BC8 was hampered. This can be attributed to the lower strain rate and temperature of ramp compression compared with shock compression. Precompressing the sample in the diamond anvil cell (DAC) and then applying

the shock wave [71] is another scheme. While this scheme is usually applied in more compressible samples [72–75]. The combination of shock compression and ramp compression is an alternative dynamic loading scheme [76–78]. Whether BC8 can be obtained under this scheme needs to be verified by future work.

In summary, we constructed a machine learning potential of high-pressure carbon fitted from first-principles calculations. The melting and Hugoniot lines calculated by this machine learning potential show good agreement with the results of our DFT calculations, as well as previous theoretical and experimental works. Using the molecular dynamics based on the machine learning potential, we designed double shock compression pathways to achieve the phase transition from diamond to BC8 carbon successfully. Diamond was first shock compressed along  $\langle 100 \rangle$  direction to 584 GPa at 20.5 km/s. Subsequently, the second shock was applied in the same direction. For the second shock, we reached a shock velocity of 24.8 or 25.0 km/s, the phase transition from diamond to BC8 can be directly observed in our nano-seconds molecular dynamics simulations. Diamond transforms into a supercooled liquid and then crystallizes to BC8. We calculated the critical nucleus size and nucleation rate of BC8 carbon, which is crucial for the observation of BC8 experimentally due to the limited observation time in dynamic compression experiments. Combining these results, we propose that the

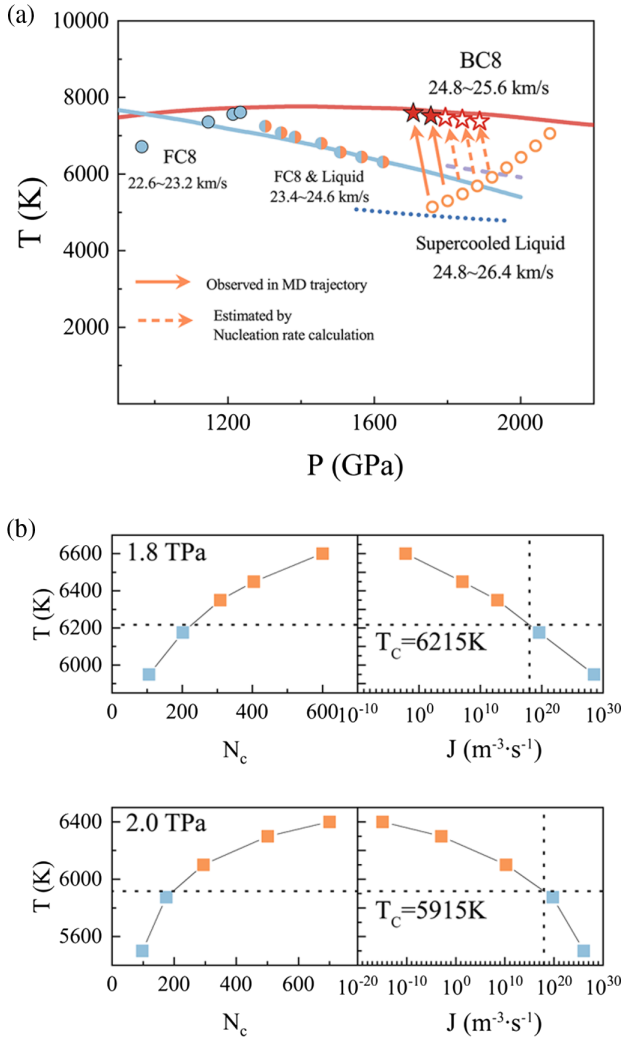


FIG. 4. The Hugoniot points of the second shock and the results of nucleation calculations. (a) The phase behaviors near the melting line of diamond and corresponding shock velocities. The melting lines of diamond and BC8 are marked as blue and red solid lines, respectively. The blue dotted line is the melting line of diamond with uniaxial strain of 0.1 along the  $\langle 100 \rangle$  direction. The purple dashed line represents the thermal condition under which the nucleation rate of BC8 is at  $1 \text{ mm}^{-3} \text{ ns}^{-1}$ . (b) The critical nucleus size ( $N_c$ ) and nucleation rate ( $J$ ) of BC8 carbon at 1.8 and 2.0 TPa, respectively. The black dashed line indicated a nucleation rate of  $1 \text{ mm}^{-3} \text{ ns}^{-1}$  and the corresponding temperature ( $T_c$ ). The temperature points below and beyond the  $T_c$  are marked as blue and orange squares, respectively.

reasonable shock velocity range for the second shock to observe the formation of BC8 is approximately from 24.8 to 25.6 km/s. We found that the key to obtaining BC8 carbon is the formation of liquid at a sufficient supercooling. Our theoretical simulations could provide insights into the phase transition from diamond to BC8 carbon and useful guidance for seeking BC8 carbon in future experiments.

J. Sun gratefully acknowledges the financial support from the National Natural Science Foundation of China

(Grants No. 12125404, No. 11974162, and No. 11834006), and the Fundamental Research Funds for the Central Universities. The calculations were carried out using supercomputers at the High Performance Computing Center of Collaborative Innovation Center of Advanced Microstructures, the high-performance supercomputing center of Nanjing University.

J. Shi and Z. L. contributed equally to this work.

\*Corresponding author: jiansun@nju.edu.cn

- [1] K. S. Novoselov, A. K. Geim, S. V. Morozov, D. Jiang, Y. Zhang, S. V. Dubonos, I. V. Grigorieva, and A. A. Firsov, Electric field effect in atomically thin carbon films, *Science* **306**, 666 (2004).
- [2] H. W. Kroto, J. R. Heath, S. C. O'Brien, R. F. Curl, and R. E. Smalley, C60: Buckminsterfullerene, *Nature (London)* **318**, 162 (1985).
- [3] S. Iijima, Helical microtubules of graphitic carbon, *Nature (London)* **354**, 56 (1991).
- [4] Q. Huang *et al.*, Nanotwinned diamond with unprecedented hardness and stability, *Nature (London)* **510**, 250 (2014).
- [5] Y. Yue *et al.*, Hierarchically structured diamond composite with exceptional toughness, *Nature (London)* **582**, 370 (2020).
- [6] H. Tang *et al.*, Synthesis of paracrystalline diamond, *Nature (London)* **599**, 605 (2021).
- [7] Y. Shang *et al.*, Ultrahard bulk amorphous carbon from collapsed fullerene, *Nature (London)* **599**, 599 (2021).
- [8] S. Zhang *et al.*, Discovery of Carbon-Based Strongest and Hardest Amorphous Material, *Natl. Sci. Rev.* **9**, nwab140 (2022).
- [9] N. Madhusudhan, K. K. M. Lee, and O. Mousis, A possible carbon-rich interior in Super-Earth 55 cancri e, *Astrophys. J.* **759**, L40 (2012).
- [10] N. Mashian and A. Loeb, CEMP stars: Possible hosts to carbon planets in the early universe, *Mon. Not. R. Astron. Soc.* **460**, 2482 (2016).
- [11] M. T. Yin and M. L. Cohen, Will Diamond Transform under Megabar Pressures?, *Phys. Rev. Lett.* **50**, 2006 (1983).
- [12] R. Biswas, R. M. Martin, R. J. Needs, and O. H. Nielsen, Stability and electronic properties of complex structures of silicon and carbon under pressure: Density-functional calculations, *Phys. Rev. B* **35**, 9559 (1987).
- [13] S. Fahy and S. G. Louie, High-pressure structural and electronic properties of carbon, *Phys. Rev. B* **36**, 3373 (1987).
- [14] C. Mailhot and A. K. McMahan, Atmospheric-pressure stability of energetic phases of carbon, *Phys. Rev. B* **44**, 11578 (1991).
- [15] S. Scandolo, G. L. Chiarotti, and E. Tosatti, SC4: A metallic phase of carbon at terapascal pressures, *Phys. Rev. B* **53**, 5051 (1996).
- [16] M. Martinez-Canales, C. J. Pickard, and R. J. Needs, Thermodynamically Stable Phases of Carbon at Multi-terapascal Pressures, *Phys. Rev. Lett.* **108**, 045704 (2012).
- [17] X. Wang, S. Scandolo, and R. Car, Carbon Phase Diagram from *Ab Initio* Molecular Dynamics, *Phys. Rev. Lett.* **95**, 185701 (2005).

- [18] A. A. Correa, S. A. Bonev, and G. Galli, Carbon under extreme conditions: Phase boundaries and electronic properties from first-principles theory, *Proc. Natl. Acad. Sci. U.S.A.* **103**, 1204 (2006).
- [19] L. X. Benedict, K. P. Driver, S. Hamel, B. Militzer, T. Qi, A. A. Correa, A. Saul, and E. Schwegler, Multiphase equation of state for carbon addressing high pressures and temperatures, *Phys. Rev. B* **89**, 224109 (2014).
- [20] A. R. Oganov, R. J. Hemley, R. M. Hazen, and A. P. Jones, Structure, bonding, and mineralogy of carbon at extreme conditions, *Rev. Mineral. Geochem.* **75**, 47 (2013).
- [21] J. Sun, D. D. Klug, and R. Martoňák, Structural transformations in carbon under extreme pressure: Beyond diamond, *J. Chem. Phys.* **130**, 194512 (2009).
- [22] A. Lazicki *et al.*, Metastability of diamond ramp-compressed to 2 terapascals, *Nature (London)* **589**, 532 (2021).
- [23] K. Nguyen-Cong, J. T. Willman, S. G. Moore, A. B. Belonoshko, R. Gayatri, E. Weinberg, M. A. Wood, A. P. Thompson, and I. I. Oleynik, Billion atom molecular dynamics simulations of carbon at extreme conditions and experimental time and length scales, in *Proceedings of the International Conference for High Performance Computing, Networking, Storage and Analysis* (ACM, St. Louis Missouri, 2021), pp. 1–12.
- [24] S. Brygoo, E. Henry, P. Loubeyre, J. Eggert, M. Koenig, B. Loupias, A. Benuzzi-Mounaix, and M. Rabec Le Gloahec, Laser-shock compression of diamond and evidence of a negative-slope melting curve, *Nat. Mater.* **6**, 274 (2007).
- [25] M. D. Knudson, M. P. Desjarlais, and D. H. Dolan, Shock-wave exploration of the high-pressure phases of carbon, *Science* **322**, 1822 (2008).
- [26] D. K. Bradley, J. H. Eggert, R. F. Smith, S. T. Prisbrey, D. G. Hicks, D. G. Braun, J. Biener, A. V. Hamza, R. E. Rudd, and G. W. Collins, Diamond at 800 GPa, *Phys. Rev. Lett.* **102**, 075503 (2009).
- [27] J. H. Eggert, D. G. Hicks, P. M. Celliers, D. K. Bradley, R. S. McWilliams, R. Jeanloz, J. E. Miller, T. R. Boehly, and G. W. Collins, Melting temperature of diamond at ultrahigh pressure, *Nat. Phys.* **6**, 40 (2010).
- [28] R. F. Smith *et al.*, Ramp compression of diamond to five terapascals, *Nature (London)* **511**, 330 (2014).
- [29] T. S. Duffy and R. F. Smith, Ultra-high pressure dynamic compression of geological materials, *Front. Earth Sci.* **7**, 23 (2019).
- [30] J. M. Winey, M. D. Knudson, and Y. M. Gupta, Shock compression response of diamond single crystals at multi-megabar stresses, *Phys. Rev. B* **101**, 184105 (2020).
- [31] K. Katagiri, N. Ozaki, Y. Umeda, T. Irifune, N. Kamimura, K. Miyanishi, T. Sano, T. Sekine, and R. Kodama, Shock Response of Full Density Nanopolycrystalline Diamond, *Phys. Rev. Lett.* **125**, 185701 (2020).
- [32] L. Bonati and M. Parrinello, Silicon Liquid Structure and Crystal Nucleation from *Ab Initio* Deep Metadynamics, *Phys. Rev. Lett.* **121**, 265701 (2018).
- [33] M. A. Caro, V. L. Deringer, J. Koskinen, T. Laurila, and G. Csányi, Growth Mechanism and Origin of High  $s p^3$  Content in Tetrahedral Amorphous Carbon, *Phys. Rev. Lett.* **120**, 166101 (2018).
- [34] B. Cheng, G. Mazzola, C. J. Pickard, and M. Ceriotti, Evidence for supercritical behaviour of high-pressure liquid hydrogen, *Nature (London)* **585**, 217 (2020).
- [35] V. L. Deringer, N. Bernstein, G. Csányi, C. Ben Mahmoud, M. Ceriotti, M. Wilson, D. A. Drabold, and S. R. Elliott, Origins of structural and electronic transitions in disordered silicon, *Nature (London)* **589**, 59 (2021).
- [36] Y. Wang, J. Wang, A. Hermann, C. Liu, H. Gao, E. Tosatti, H.-T. Wang, D. Xing, and J. Sun, Electronically Driven 1D Cooperative Diffusion in a Simple Cubic Crystal, *Phys. Rev. X* **11**, 011006 (2021).
- [37] J. T. Willman, K. Nguyen-Cong, A. S. Williams, A. B. Belonoshko, S. G. Moore, A. P. Thompson, M. A. Wood, and I. I. Oleynik, Machine learning interatomic potential for simulations of carbon at extreme conditions, *Phys. Rev. B* **106**, L180101 (2022).
- [38] B. Cheng, S. Hamel, and M. Bethkenhagen, Thermodynamics of diamond formation from hydrocarbon mixtures in planets, *Nat. Commun.* **14**, 1104 (2023).
- [39] Z. Fan *et al.*, GPUMD: A package for constructing accurate machine-learned potentials and performing highly efficient atomistic simulations, *J. Chem. Phys.* **157**, 114801 (2022).
- [40] See Supplemental Material at <http://link.aps.org/supplemental/10.1103/PhysRevLett.131.146101> for more details about the DFT calculation, the construction of MLP, the validation test of MLP, the method to recognize atomic environment, the MD simulations using the MLP, and the detailed discussions of Fig. 4(a), which includes Refs. [41–57].
- [41] G. Kresse and J. Furthmüller, Efficient iterative schemes for *ab initio* total-energy calculations using a plane-wave basis set, *Phys. Rev. B* **54**, 11169 (1996).
- [42] P. E. Blöchl, Projector augmented-wave method, *Phys. Rev. B* **50**, 17953 (1994).
- [43] J. P. Perdew, K. Burke, and M. Ernzerhof, Generalized Gradient Approximation Made Simple, *Phys. Rev. Lett.* **77**, 3865 (1996).
- [44] S. Nosé, A unified formulation of the constant temperature molecular dynamics methods, *J. Chem. Phys.* **81**, 511 (1984).
- [45] W. G. Hoover, Canonical dynamics: Equilibrium phase-space distributions, *Phys. Rev. A* **31**, 1695 (1985).
- [46] B. Cheng *et al.*, Mapping materials and molecules, *Acc. Chem. Res.* **53**, 1981 (2020).
- [47] S. De, A. P. Bartók, G. Csányi, and M. Ceriotti, Comparing molecules and solids across structural and alchemical space, *Phys. Chem. Chem. Phys.* **18**, 13754 (2016).
- [48] A. P. Bartók, S. De, C. Poelking, N. Bernstein, J. R. Kermode, G. Csányi, and M. Ceriotti, Machine learning unifies the modeling of materials and molecules, *Sci. Adv.* **3**, e1701816 (2017).
- [49] L. Himanen, M. O. J. Jäger, E. V. Morooka, F. Federici Canova, Y. S. Ranawat, D. Z. Gao, P. Rinke, and A. S. Foster, Dscribe: Library of descriptors for machine learning in materials science, *Comput. Phys. Commun.* **247**, 106949 (2020).
- [50] M. Bernetti and G. Bussi, Pressure control using stochastic cell rescaling, *J. Chem. Phys.* **153**, 114107 (2020).

- [51] A. B. Belonoshko, R. Ahuja, and B. Johansson, Quasi-*Ab Initio* Molecular Dynamic Study of Fe Melting, *Phys. Rev. Lett.* **84**, 3638 (2000).
- [52] J. R. Morris and X. Song, The melting lines of model systems calculated from coexistence simulations, *J. Chem. Phys.* **116**, 9352 (2002).
- [53] E. R. Hernández, A. Rodríguez-Prieto, A. Bergara, and D. Alfè, First-Principles Simulations of Lithium Melting: Stability of the Bcc Phase Close to Melting, *Phys. Rev. Lett.* **104**, 185701 (2010).
- [54] M. I. Mendeleev, M. J. Kramer, C. A. Becker, and M. Asta, Analysis of semi-empirical interatomic potentials appropriate for simulation of crystalline and liquid Al and Cu, *Philos. Mag.* **88**, 1723 (2008).
- [55] S. Auer and D. Frenkel, Numerical prediction of absolute crystallization rates in hard-sphere colloids, *J. Chem. Phys.* **120**, 3015 (2004).
- [56] A. Widmer-Cooper, P. Harrowell, and H. Fynewever, How Reproducible Are Dynamic Heterogeneities in a Supercooled Liquid?, *Phys. Rev. Lett.* **93**, 135701 (2004).
- [57] A. B. Belonoshko, N. V. Skorodumova, A. Rosengren, and B. Johansson, Melting and critical superheating, *Phys. Rev. B* **73**, 012201 (2006).
- [58] A. B. Belonoshko, Molecular dynamics of MgSiO<sub>3</sub> perovskite at high pressures: Equation of state, structure, and melting transition, *Geochim. Cosmochim. Acta* **58**, 4039 (1994).
- [59] F. Soubiran and B. Militzer, Anharmonicity and Phase Diagram of Magnesium Oxide in the Megabar Regime, *Phys. Rev. Lett.* **125**, 175701 (2020).
- [60] F. González-Cataldo, B. K. Godwal, K. Driver, R. Jeanloz, and B. Militzer, Model of ramp compression of diamond from *ab initio* simulations, *Phys. Rev. B* **104**, 134104 (2021).
- [61] E. J. Reed, L. E. Fried, and J. D. Joannopoulos, A Method for Tractable Dynamical Studies of Single and Double Shock Compression, *Phys. Rev. Lett.* **90**, 235503 (2003).
- [62] E. J. Reed, A. Maiti, and L. E. Fried, Anomalous sound propagation and slow kinetics in dynamically compressed amorphous carbon, *Phys. Rev. E* **81**, 016607 (2010).
- [63] Y. Shen, S. B. Jester, T. Qi, and E. J. Reed, Nanosecond homogeneous nucleation and crystal growth in shock-compressed SiO<sub>2</sub>, *Nat. Mater.* **15**, 60 (2016).
- [64] J. R. Espinosa, C. Vega, C. Valeriani, and E. Sanz, Seeding approach to crystal nucleation, *J. Chem. Phys.* **144**, 034501 (2016).
- [65] J. R. Espinosa, C. Vega, C. Valeriani, and E. Sanz, The crystal-fluid interfacial free energy and nucleation rate of NaCl from different simulation methods, *J. Chem. Phys.* **142**, 194709 (2015).
- [66] H. Niu, L. Bonati, P. M. Piaggi, and M. Parrinello, *Ab initio* phase diagram and nucleation of gallium, *Nat. Commun.* **11**, 1 (2020).
- [67] P. M. Piaggi, J. Weis, A. Z. Panagiotopoulos, P. G. Debenedetti, and R. Car, Homogeneous ice nucleation in an *ab initio* machine learning model of water, *Proc. Natl. Acad. Sci. U.S.A.* **119**, e2207294119 (2022).
- [68] L. E. Hansen *et al.*, Melting of magnesium oxide up to two terapascals using double-shock compression, *Phys. Rev. B* **104**, 014106 (2021).
- [69] Y. Ping *et al.*, Solid Iron Compressed Up to 560 GPa, *Phys. Rev. Lett.* **111**, 065501 (2013).
- [70] M. Millot, F. Coppari, J. R. Rygg, A. Correa Barrios, S. Hamel, D. C. Swift, and J. H. Eggert, Nanosecond x-ray diffraction of shock-compressed superionic water ice, *Nature (London)* **569**, 251 (2019).
- [71] R. Jeanloz, P. M. Celliers, G. W. Collins, J. H. Eggert, K. K. M. Lee, R. S. McWilliams, S. Brygoo, and P. Loubeyre, Achieving high-density states through shock-wave loading of precompressed samples, *Proc. Natl. Acad. Sci. U.S.A.* **104**, 9172 (2007).
- [72] K. K. M. Lee *et al.*, Laser-driven shock experiments on precompressed water: Implications for “Icy” giant planets, *J. Chem. Phys.* **125**, 014701 (2006).
- [73] M. Millot, S. Hamel, J. R. Rygg, P. M. Celliers, G. W. Collins, F. Coppari, D. E. Fratanduono, R. Jeanloz, D. C. Swift, and J. H. Eggert, Experimental evidence for superionic water ice using shock compression, *Nat. Phys.* **14**, 297 (2018).
- [74] L. E. Crandall, J. R. Rygg, D. K. Spaulding, T. R. Boehly, S. Brygoo *et al.*, Equation of State of CO<sub>2</sub> Shock Compressed to 1 TPa, *Phys. Rev. Lett.* **125**, 165701 (2020).
- [75] Y.-J. Kim *et al.*, Evidence for Dissociation and Ionization in Shock Compressed Nitrogen to 800 GPa, *Phys. Rev. Lett.* **129**, 015701 (2022).
- [76] M. D. Knudson, M. P. Desjarlais, A. Becker, R. W. Lemke, K. R. Cochrane, M. E. Savage, D. E. Bliss, T. R. Mattsson, and R. Redmer, Direct observation of an abrupt insulator-to-metal transition in dense liquid deuterium, *Science* **348**, 1455 (2015).
- [77] A. Krygier, P. D. Powell, J. M. McNaney, C. M. Huntington, S. T. Prisbrey *et al.*, Extreme Hardening of Pb at High Pressure and Strain Rate, *Phys. Rev. Lett.* **123**, 205701 (2019).
- [78] R. G. Kraus *et al.*, Measuring the melting curve of iron at super-earth core conditions, *Science* **375**, 202 (2022).
- [79] P. M. Larsen, S. Schmidt, and J. Schiøtz, Robust structural identification via polyhedral template matching, *Model. Simul. Mater. Sci. Eng.* **24**, 055007 (2016).
- [80] A. Stukowski, Visualization and analysis of atomistic simulation data with OVITO—the open visualization tool, *Model. Simul. Mater. Sci. Eng.* **18**, 015012 (2010).